ELSEVIER

Journal of Nuclear Materials 306 (2002) 73–77

journal of nuclear materials

www.elsevier.com/locate/jnucmat

Observations of hydrocarbon film deposition in the MAST tokamak

A. Tabasso [a,*], G.F. Counsell [a], D. Hole [b], J.P. Coad [a]

[a] *Culham Science Centre, Euratom/UKAEA Fusion Association, Abingdon, Oxon OX 14 3DB, UK*
[b] *School of Engineering, University of Sussex, Brighton BN1 9QH, UK*

Received 18 April 2002; accepted 15 July 2002

Abstract

Two divertor tiles from the Mega-Ampere Spherical Tokamak (MAST) were analysed using interference fringe analysis, nuclear reaction analysis and Rutherford backscattering analysis. The analysis allowed the quantification of the co-deposited layers thickness of the deuterium and carbon mixture and the detection of the presence of other impurities such as oxygen and iron. A layer thickness varying from 10 to 270 nm was measured with a typical $D/(D+C)$ ratio of $\approx$0.36. During the same campaign in which the analysed divertor tiles were exposed to the plasma, the ion flux to the divertor plates has been measured by a set of Langmuir probes mounted on the divertor ribs. This paper shows that the sputtering co-efficient that can be inferred from the ion fluences measured by the probes and by the redeposition of C in those amorphous layers is consistent with physical and chemical sputtering yields in conventional tokamaks. This paper reports the beginning and the intended developments of a project undertaken in MAST to study and quantify the phenomena of plasma surface interaction both at the walls and at the divertor of the machine in order to contribute to the material choice and design of the plasma facing components of a next step device such as ITER.

1. Introduction

Carbon, as CFC, is the favoured material for the ITER strike point region. It is therefore important to understand the erosion and redeposition mechanisms for carbon in existing machines to better understand issues affecting both target lifetime and impurity contamination of the plasma. EK986 graphite plasma facing components removed from the Mega-Ampere Spherical Tokamak (MAST) divertor following the first operational campaign clearly show the accumulation of co-deposited hydrocarbon films. These components were in a clean, vacuum baked state before installation prior to the first MAST campaign. They experienced only a relatively limited range of plasma scenarios before their removal, making the post-mortem surface analysis an easier task.

MAST is equipped with a set of 12 upper and 12 lower divertor ribs as illustrated in Fig. 1. Each rib consists of 3 EK986 graphite divertor tiles onto which the outer strike point plasma sweeps. This natural sweep is due to the solenoid fringing and each MAST discharge sees the outer strike points moving outwards and the inner strike points moving upwards (the lower one) and downwards (the upper one) from the X point formation to the end of the discharge. Each outer strike point tile is $\approx$31 cm long and 16 cm wide. As one can see in the figure, two of the ribs are wider because the Langmuir probes and thermocouples are installed in these ribs. The inner strike point rests on graphite protection tiles on the top and bottom of the centre column.

* Corresponding author. Tel.: +44-1235 466528; fax: +44-1235 464192.
E-mail address: alberto.tabasso@ukaea.org.uk (A. Tabasso).

0022-3115/02/$ - see front matter
PII: S0022-3115(02)00936-4

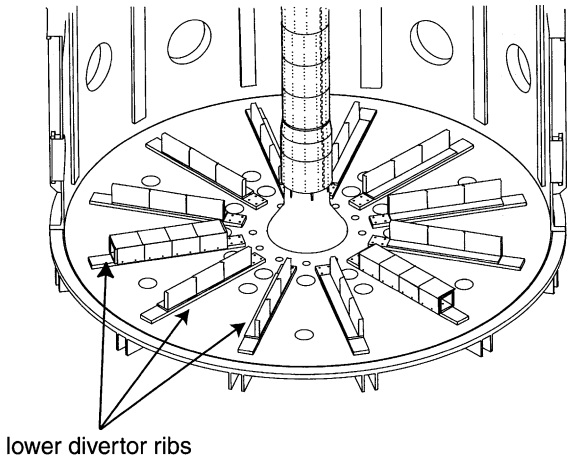

Fig. 1. Schematic of MAST lower divertor ribs.

Because the magnetic field lines intercept the horizontal face of the target ribs at a shallow angle (typically between 7° and 13° to the horizontal, varying with major radius), each tile shadows a portion (typically more than half) of the following tile (see Fig. 2). Moreover, since the directions of the toroidal field and plasma current were unchanged, only one toroidal face (the *leading* face) of each rib was exposed to the strike point, with the second (*trailing*) face and the vessel end plate between the ribs being shadowed.

Clear signs of arcing are present on the plasma wetted area, they are rather shallow and no pitting is present on the tile (see Fig. 3) which shows the top part of both the leading and trailing face of the middle divertor tile and a small portion of the inner and outer ones. Inspection of the arcing damage shows the very sporadic and localised nature of the erosion and redeposition of these events.

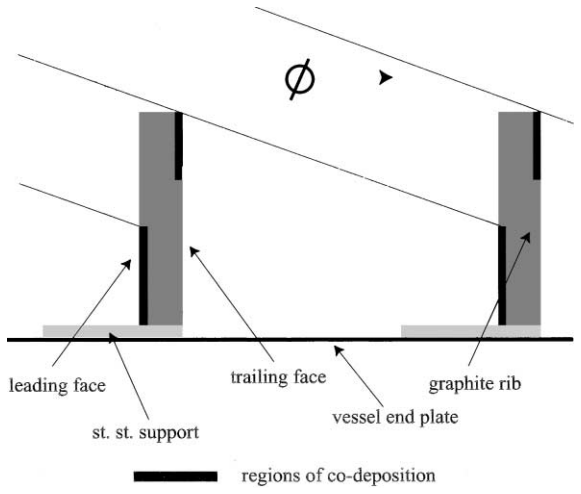

Fig. 2. Schematic showing regions of field line shadowing and co-deposition on the MAST divertor tiles.

Film formation, due to the redeposition of the carbon eroded by the divertor plasma ions, was observed in the shadowed regions on both sides of the rib (Fig. 3). There was, however, no apparent deposition either on the stainless steel supports for the ribs or on the stainless steel vessel end plates. The films on ribs from the upper and lower divertor appeared visually very similar and components from the lower divertor were analysed in detail. In addition, only the two tiles comprising the outer two thirds of one of these ribs, covering the outer divertor region $\approx 1.0\ \text{m} < R <\approx 1.6\ \text{m}$, were removed for analysis. The tiles have been exposed for a total divertor double null operation of ≈185 s.

2. Experimental method

The MAST divertor tiles were inserted in the machine in a clean (oil-free machined and further cleaned in ultrasonic bath of demineralised water first and of isopropanol afterwards), vacuum baked state (2 h at ≈150 °C in air and 1 h at 450 ° C in vacuum), before the beginning of the campaign and were removed after a rather limited period of plasma operation.

Two tiles were selected for the analysis of the distribution and composition of the co-deposited film: the lower divertor centre and outer tiles. Because the tiles presented a rather simple interference pattern (only the second order interference fringes were visible), it was considered not necessary to proceed with a full colourimetry analysis [1]. It was therefore decided to apply a simple interference fringe analysis (IFA) on the samples in order to assess the thickness of those layers. Hence IFA [2] was performed on these tiles at two radial positions. The IFA was carried out along the z-axis (see Fig. 4). The conditions under which the analysis was performed were the following: daylight (D65, colour temperature 6500 K), colours observed by human eyes at $\theta = 0°$, i.e. perpendicularly to the target. A refractive index $n = 2$ was assumed [1], which is consistent with the average of that reported on deposited amorphous C and D films in [3] within ≈15%. An absorption co-efficient $\kappa \approx 0.01$ was also assumed; this is again typical for these kind of films on graphite [1]. The outer tile was then cut in four strips along the z direction and each sample was analysed with nuclear reaction analysis (NRA) and Rutherford backscattering analysis (RBS) (see Fig. 4).

The four strips cut from the outer tile were analysed with a 0.8 MeV He^3 ion beam and on the same spot both NRA and RBS were performed. The analysis was performed using a 3.0 MeV ion beam van der Graaff linear accelerator and a dedicated analysis chamber [4]. Typically about 10 spots were analysed in each strip. From the NRA we expected to learn about the amount of D present in the layers while from RBS we wanted to establish the concentration of the materials in the layers and the presence of impurities.

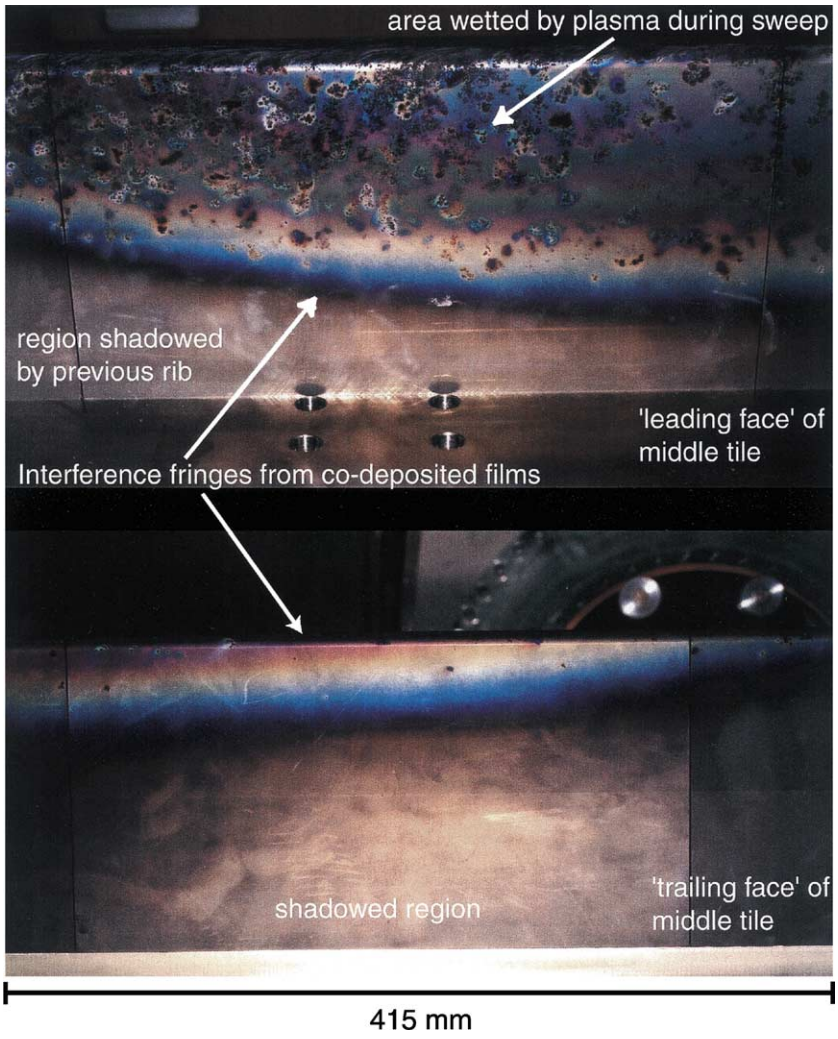

Fig. 3. Photographs of the leading (upper) and trailing (lower) face of the middle rib tile showing regions of co-deposit formation. Also noticeable on the upper image is the arc damage to the wetted region of the leading face.

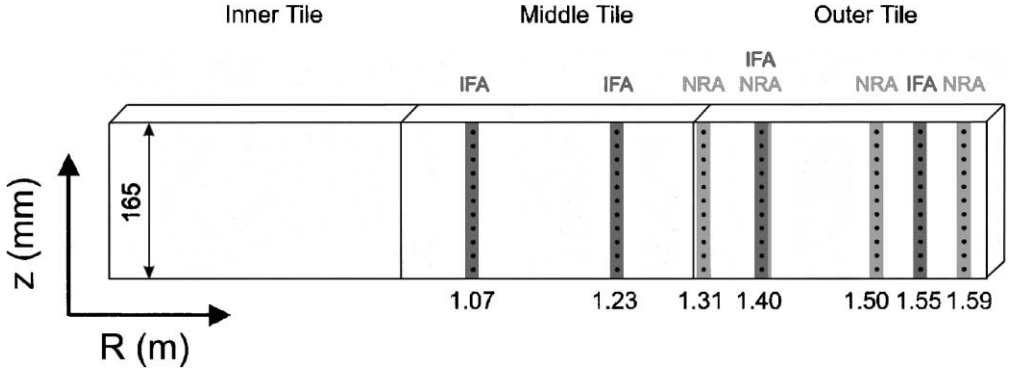

Fig. 4. Schematic showing the three lower outer divertor tiles and the locations of the IFA and NRA (together with RBS) analysis.

Having measured the amount of redeposited material it was then possible to estimate the amount of erosion that would correspond to such deposition. MAST is equipped with arrays of flush mounted, target Langmuir probes covering the four strike point regions [5]. At the outer strike points the arrays are embedded in the horizontal face of one of the divertor ribs, at a toroidal location 120° from the position of the rib from which the tiles were removed. The probes have a spatial resolution of 10 mm and are swept once every 3 ms. Since the typical power deposition width at the targets is (10 ± 2) cm, the probes are able to provide a good estimate of instantaneous target conditions. It was therefore possible to calculate the ion fluence to the target and relate it to the amount of measured sputtering material to thereby drawing conclusions on the typical MAST sputtering co-efficients averaged over a whole campaign.

3. Results

Fig. 5 shows a survey of the measured thickness of the film on the leading face of the middle and outer tiles using IFA. The abscissa represents the vertical direction from the bottom of the tile to the top. Four radial positions are plotted: 1.07, 1.23, 1.40 and 1.55 m (see Fig. 4). The film thickness consistently peaks at around 250 nm close to the boundary of the shadowed region. The fact that the refractive index and absorption co-efficient of the film are inferred rather than known may introduce an uncertainty in this measurement of as much as 10%. Allowing for the effect of the natural sweeping of the strike points, this film thickness corresponds to a peak deposition rate of 2–3 nm/s. The film halved in thickness within 6 cm below the shadow boundary on the leading face and in a much shorter distance, within 2 cm from the top of the rib, on the trailing face.

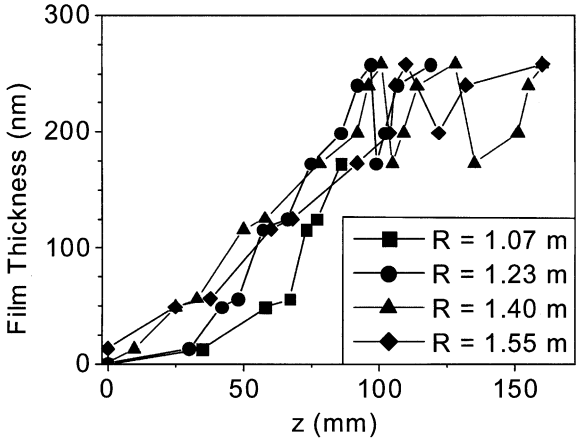

Fig. 5. IFA measurements of the film thickness on the leading face of the middle ($1.0\ \text{m} < R < 1.3$ m) and outer ($1.3\ \text{m} < R < 1.6$ m) tiles, as a function of vertical height up the tile.

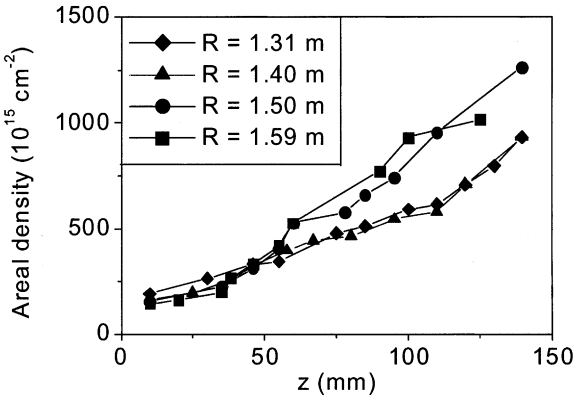

Fig. 6. NRA measurements of the areal deuterium density D in films on the outer tile as a function of vertical (poloidal) height and major radius.

Fig. 6 shows the vertical (poloidal) profiles of the deuterium areal density in the films at four radial locations ($R \approx 1.31$, 1.40, 1.50 and 1.59 m) on the leading face of the outer tile, as measured with NRA (see Fig. 4). Note that two radial locations on the tile are very close to the locations where IFA was performed. A typical deuterium areal density close to the shadow boundary was determined to be 1040×10^{15} cm^{-2}. Using the average deuterium atomic density for the films in [4] of $\approx 4 \times 10^{22}$ cm^{-3} (corresponding to a $D/(D+C)$ ratio of ≈ 0.36 and density of 1.6 g/cm^3, with $n = 2.0$ as used in the IFA [3]) leads to an estimate of the MAST film thickness close to the shadow boundary of 253 nm, in quite good agreement with that derived from IFA.

In Fig. 7 it is shown a typical RBS spectrum of a point on the tile closest to the shadow boundary (i.e.

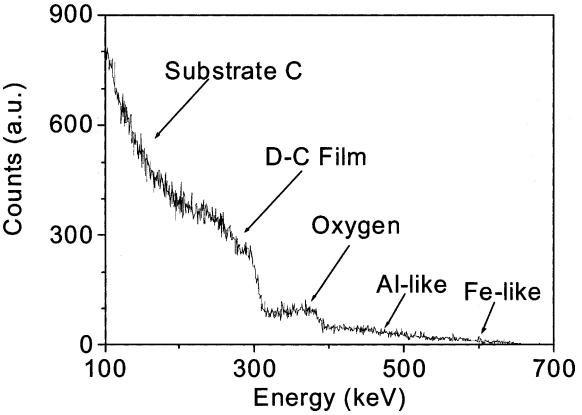

Fig. 7. Typical RBS spectrum from near the shadow boundary at $R \approx 1.02$ m annotated with probable impurity composition.

where the film thickness is highest) at $R \approx 1.02$ m. Unfortunately, surface roughness of the tile combined with local arc damage to the films (see Fig. 3) and boron deposition (from occasional boronisation during the first MAST campaign) made the spectrum difficult to fit. As a result, although the analysis did reveal the presence of Fe-like, Al-like and oxygen impurities in the co-deposited films, it was not possible to derive the $D/(D+C)$ ratio or film thickness from this measurement.

In order to relate the film thickness to erosion and redeposition in the MAST divertor the ion flux measured by the Langmuir probes was used. The average peak ion flux measured by the probes, which varied little between ohmic and L-mode phases, was ≈ 2.5 kA/m^2 with a typical electron temperature of around 10eV. Adjusting for the field line angle of incidence between the horizontal and vertical rib surfaces, the typical peak ion flux on the leading face was therefore ≈ 14 kA/m^2. The average ion flux over the region of the strike point sweep (0.5–0.7 m in length) was around 2 kA/m^2, which corresponds to a deuterium ion flux of $\approx 1.3 \times 10^{22}$ m^{-2}/s. This is of course a rather crude approximation, it will, however, allow the ion fluence to the divertor to be inferred and in turn the consistency of the derived sputtering yields to be checked. The total D^+ rate to the wetted region of the leading face on the outer tile ($1.3 \text{ m} < R < 1.6$ m) (about 0.013 m^2) was therefore $(1.7 \pm 0.8) \times 10^{20}$ s^{-1} or a fluence of $(3.4 \pm 1.6) \times 10^{22}$ m^{-2}, integrated over the whole campaign.

From the IFA and NRA, the total carbon inventory in the co-deposited films on the outer tile was estimated at $\approx 3.7 \times 10^{20}$ C atoms. This estimate is based on the fall-off length of the thickness of those films measured by IFA on the outer tile and on the portion of the tile area on which they are present. Although the transport of eroded carbon to the co-deposited region of the ribs remains to be determined, all the ribs showed rather similar patterns of deposition. The average integrated ion flux and carbon inventory could then be used to estimate a minimum total carbon erosion yield on the leading face of the ribs of $\gamma = (1.1 \pm 0.55)\%$. This is consistent with the physical and chemical erosion yields in [6] for room temperature carbon being bombarded by deuterium ions in the energy range 10–30 eV and fluxes of the order 10^{22} m^{-2}/s, which are around 0.7–1% and 0.8–2%, respectively, for physical only and physical and chemical erosion.

4. Conclusion

EK986 graphite divertor ribs, removed after the first MAST campaign, show co-deposited hydrocarbon films up to 250 nm thick in the regions of the ribs shadowed from the plasma, corresponding to an effective deposition rate of 2–3 nm/s. From NRA, the average deuterium areal density in these films, close the region of the ribs shadowed from the plasma, is $\approx 1040 \times 10^{15}$ cm^{-2} and from consistency between the NRA and IFA and using the data in [4], the average D/C ratio is estimated as ≈ 0.36.

From Langmuir probe measurements, although the error in the measurement is quite large, the average peak deuterium ion rate to the wetted area on the leading face of the outer rib tile is $(1.7 \pm 0.8) \times 10^{20}$ s^{-1}, with a fluence of $(3.4 \pm 1.6) \times 10^{22}$ m^{-2} over the campaign. Comparing this to the total carbon inventory in the films, of $\approx 3.7 \times 10^{20}$ atoms, leads to a minimum estimate for total carbon erosion yield on the leading face of the ribs of $\gamma = (1.1 \pm 0.55)\%$, consistent with that observed in other tokamaks and showing that MAST can be used for erosion/deposition studies.

Future work will include modelling of carbon transport in the toroidally asymmetric MAST divertor environment, initially using the DIVIMP/EIRENE code, which is being implemented for the MAST SOL [7]. The very large impurity ion gyro-radii (typically >1 cm) resulting from the low field in the divertor region ($B_\phi \sim 0.2$ T typical) are expected to play a key role. Additional diagnostics, including ASDEX type shuttered long term samples [8], have already been installed in the MAST vessel and their analysis will assist in validation of the modelling. The installation of a quartz crystal microbalance for real-time measurement of co-deposition and erosion/deposition markers in the tiles is also being considered.

Acknowledgements

This work is jointly funded by Euratom and the UK Department of Trade and Industry. The authors would also like to gratefully acknowledge the help of P. Wienhold of IPP – Jülich in the IFA analysis.

References

[1] P. Wienhold, private communication, March 2001.
[2] P. Wienhold, F. Weschenfelder, J. Winter, Nucl. Instrum. and Meth. 94 (1998) 503.
[3] T. Schwarz-Selinger, A. von Keudell, W. Jacob, J. Appl. Phys. 86 (1999) 3988.
[4] J.C.B. Simpson, H. Bergsaker, S. Clement, J.P. Coad, L. de Kock, J. Ehrenberg, C.J. Hancock, J.F. Neill, J. Partridge, J.E. Vince, Nucl. Instrum. and Meth. 40&41 (1989) 842.
[5] G.F. Counsell, J.W. Ahn, 27th EPS Conf. on Contr. Fus. and Plasma Phys., ECA Vol. 24, 2000.
[6] J. Roth, J. Nucl. Mater. 266–269 (1999) 51.
[7] A. Kirk, J.W. Ahn, D. Coster, G.F. Counsell, W. Fundamenski, 28th EPS Conf. on Contr. Fus. and Plasma Phys., ECA Vol. 25, 2001.
[8] A. Tabasso, J. Roth, H. Meier, K. Krieger, The ASDEX Upgrade Team, 26th EPS Conf. on Contr. Fus. and Plasma Phys., ECA Vol. 23, 1999.